Volume 1 | Number 1 | Jan 2013 | Pages 1–100

Nanoscale

www.rsc.org/nanoscale

ROYAL SOCIETY OF CHEMISTRY

www.rsc.org/nanoscale

Journal Name

ARTICLE

R2R-printed inverted OPV modules – towards arbitrary patterned designs

M. Välimäki *[a], P. Apilo [a], R. Po [b], E. Jansson [a], A. Bernardi [b], M. Ylikunnari [a], M. Vilkman [a], G. Corso [b], J. Puustinen [c], J. Tuominen [a], and J. Hast [a]

We describe the fabrication of roll-to-roll (R2R) printed organic photovoltaic (OPV) modules using gravure printing and rotary screen-printing processes. These two-dimensional printing techniques are differentiating factor from coated OPVs enabling the direct patterning of arbitrarily shaped and sized features into visual shape and, increasing the freedom to connect the cells in modules. The inverted OPV structures comprise five layers that are either printed or patterned in an R2R printing process. We examined the rheological properties of the inks used and their relation to printability, the compatibility between the processed inks, and the morphology of the R2R-printed layers. We also evaluate the dimensional accuracy of the printed pattern, which is an important consideration in designing arbitrarily-shaped OPV structures. The photoactive layer and top electrode exhibited excellent cross-dimensional accuracy corresponding to the designed width. The transparent electron transport layer extended 300 μm beyond the designed values, whereas the hole transport layer shrank 100 μm. We also examined the repeatability of the R2R fabrication process when the active area of the module varied from 32.2 cm^2 to 96.5 cm^2. Thorough layer-by-layer optimization of the R2R printing processes resulted in realization of R2R-printed 96.5-cm^2 sized modules with a maximum power conversion efficiency of 2.1% (mean 1.8%) processed with high functionality.

Introduction

The Organic solar cells, constructed with solution-processed polymers and fullerenes, are a promising disruptive technology for affordable, sustainable, and decentralized energy production. Since the discovery of organic photovoltaics (OPV) in the 1980s, extensive research efforts have focused on improving the power conversion efficiency (PCE) beyond 10%.[1-3] To date, the use of high performance photoactive materials has provided PCEs approaching 11%.[4] These small area record cells are usually processed with energy-intensive or non-scalable techniques, however, such as vacuum evaporation and spin coating, often on glass substrates under inert conditions.[5-8] On the other hand, with large-area roll-to-roll (R2R) modules processed in air using conventional materials such as poly(3-hexylthiophene):[6,6]-phenyl C61 butyric acid methyl ester (P3HT:PCBM), PCEs are produced in the range of only 2% to 3%.[9] There are several reasons for this performance gap:[10-13] (i) fundamental issues related to the dimension of the elementary cell; (ii) final synthetic

accessibility and cost of the materials; and (iii) the current lack of ink formulations that are applicable for R2R processing techniques, which limits the range of materials transferable from the laboratory to the pilot and further to industrial scale.[10-15] Indeed, the device behavior is greatly affected by the active layer morphology, which in turn depends on both the selected deposition technique, and the post-treatment and deposition conditions.[16-20] Ink formulations for all layers must be re-optimized to achieve the proper rheological properties as well as the ideal nano- and micromorphologies with consideration of the chemical compatibility and wetting issues of the overlapping layers. Importantly, the laboratory scale fabrication of solar cells does not actually indicate the technical feasibility or the economic sustainability of flexible OPV technology, as often claimed in the literature; that is, real PV modules for commercial applications on flexible substrates must be fabricated using an R2R process.[21]

Slot-die coating is the most often used and well-established technique for R2R manufacturing of OPV modules.[22-32] The key advantage of slot die coating is that there are no strict limitations on the properties of the coating inks. Inks with a wide viscosity and solids content range can be successfully coated.[22] Krebs et al. demonstrated the possibility to manufacture ITO-free modules, with all-R2R-processed layers, and the outstanding potential of OPV by building solar parks.

[a.] VTT Technical Research Centre of Finland Kaitoväylä 1, FIN-90571 Oulu, Finland E-mail: Marja.Valimaki@vtt.fi
[b.] ENI S.p.A Research Center for non-Conventional Energies Istituto ENI Donegani, Novara, Italy
[c.] University of Oulu, Microelectronics and Materials Physics Laboratories, PO BOX 4500, 90014 University of Oulu (Finland)

[30-31] The major limitation of the slot-die process, however, is its patterning capability, which limits the pattern shape to stripes. From digital printing processes, inkjet printing is a technique that enables customized OPV cells and modules.[26-27,33-35] In contrast, mechanical printing technologies, such as gravure printing, flexography printing, screen printing, and offset printing have the advantage of large-area arbitrary shape and size processing using additive R2R process steps in a sequence. This increases the freedom of product design and its integration into various applications. The potential of gravure printing as an OPV manufacturing technique has been demonstrated in small area cells and modules in laboratory scale, and in a sheet-to-sheet industrial scale process.[36-41] Some groups have also reported R2R gravure-printed conventional cells and modules.[18-19,42] These fabrication processes, however, still involve an evaporation step. Hübler *et al.* reported the deposition of R2R-printed small-area OPV cells on a paper substrate by a combination of flexography and gravure printing for preparation of the devices.[43]

In the present study, we describe R2R-printed inverted OPV modules created using gravure printing and rotary screen printing techniques. Here we focused on R2R processing of an indium tin oxide (ITO)-zinc oxide (ZnO)-P3HT:PCBM-poly(3,4-ethylenedioxythiophene):poly(styrenesulfonate) (PEDOT:PSS)-silver structure in terms of printability and patterning. We have used only printing methods to manufacture OPV modules except sputtered ITO-PET is employed as a basis. ITO can be replaced for instance with transparent/semi-transparent conducting materials[44-45] i.e. printed metal grid and PEDOT:PSS[46-52], coated silver nanowires[53] for further cost reductions. First, we discuss the rheological properties of the inks used and their relation to printability. Furthermore, we investigated the morphology of the R2R-printed layers. Second, we performed compatibility tests prepared with four different silver pastes in laboratory scale. Third, we examined the spreading of the inks, i.e., the accuracy of the printed pattern and registration in the R2R process in a cross-machine direction (CD). Fourth, we investigated the electrical performance and repeatability of the R2R-printed modules throughout the run with varying module sizes. Finally, we provide a summary of the results with concluding remarks, and a description of the module preparation and characterization in the Experimental section.

2. Results and discussion

2.1. R2R process

The inverted OPV structure investigated in this work comprised a total of five layers that are either printed or patterned in an separate R2R process steps (Figure 1). As a first process step, ITO is patterned as a negative image using rotary screen printing to define the desired pattern.[54] Next, ZnO, which acts as an electron transport layer, is R2R gravure-printed. The gravure printing of ZnO is described in a separate article.[55] The photoactive layer of P3HT:PCBM is also R2R

gravure printed.[42] We used PEDOT:PSS as the hole transport layer and silver ink as the hole contact, both printed with the R2R rotary screen printing process. The printing methods were selected based on the properties of the selected material and the targeted layer thickness. The etching paste for ITO, PEDOT:PSS grade and silver paste were developed for flat-bed screen printing, and thus the rotary screen printing was selected for R2R processing. Moreover, the lower viscosity of the ZnO and P3HT:PCBM inks favors the use of gravure printing in their deposition, allowing for construction of the desired layer thickness of tens or hundreds of nanometers in the OPV cell structure. Details of the materials, inks/pastes, and processing are provided in the Experimental section.

2.2. Rheological properties and printability of R2R-printed layers

The rheological properties are crucial for obtaining good uniformity and well-defined edges in the R2R-printed layers. The rheological properties of the PEDOT:PSS and P3HT:PCBM inks and their relation to printability were investigated. The viscosity values of PEDOT:PSS and P3HT:PCBM at different shear rates are shown in Figure 2. Both of the inks are shear-thinning and the thinning behavior is very rapid, which is beneficial in the printing processes. As a screen printing paste, the viscosity of PEDOT:PSS ink is significantly higher than that of the P3HT:PCBM ink for gravure printing. During the printing process, the PEDOT:PSS and P3HT:PCBM ink viscosities are approximately 600 mPa•s and 25 mPa•s, respectively. Higher shear rates cannot be measured with the equipment used, but it should be noted that shear rate can exceed values up to 100 000 s^{-1} in gravure printing.[56] The thixotropy and amplitude sweep curves of PEDOT:PSS and P3HT:PCBM are also shown in Figure 2. The high flow point (>> 10%) and fast viscosity recovery after the high shear load of the PEDOT:PSS ink indicates that the ink might have some leveling issues on the substrate during printing. This ink also has significant gel-like behavior (G' > G'') at low strain values, which leads to an uneven ink distribution within the printed layers. P3HT:PCBM ink has a lower flow point, which facilitates the formation of uniform layers. The P3HT:PCBM ink viscosity recovers rather quickly after the high shear load, but not to the same level as before shearing, which indicates that the ink layer has a different structure (polymer matrix structure and orientation) than before printing and that the ink distribution within the printed layer might be uneven.

As described earlier, the rheological measurement of P3HT:PCBM ink predicts good leveling of the ink layer, but the blend of two different materials in the ink might cause some unevenness in the material distribution within the printed layer. Gravure printing of the P3HT:PCBM layer, however, provided excellent control of the ink and a uniform layer with a thickness of 175 (±12) nm on top of the ZnO layer in the R2R process.

Nanoscale Accepted Manuscript

The rheology measurement indicates limited leveling and distribution of PEDOT:PSS in printing. Furthermore, the aqueous dispersion of PEDOT:PSS cannot provide good printing quality directly on top of the hydrophobic surface of P3HT:PCBM. Various strategies can be used to improve the printability, which involve the addition of co-solvents and/or additives to the PEDOT:PSS or pre-treatment of the P3HT:PCBM surface with plasma/corona or solvents. Generally, the addition of a suitable co-solvent improves the leveling and distribution of the ink, but even minor additions of co-solvent remarkably change the rheological behavior of PEDOT:PSS paste.[57] Surfactants, such as Triton X-100, Zonyl FS-300, and Capstone FS-31 have been used to enhance the surface properties of PEDOT:PSS; thus, most studies have focused on improving the wettability of PEDOT:PSS.[39-40, 58] Surfactants might lead to lower cell performance and/or shortened lifetime, and extensive studies are required to confirm their device compatibility. Lim *et al.* reported that the use of Capstone FS-31 with PEDOT:PSS improves the wettability while maintaining a device efficiency of 3.1%, and even increases the device lifetime.[58] The surface treatment of P3HT:PCBM with plasma or corona increase the surface energy of P3HT:PCBM, but has detrimental effects on the device performance. The wetting and leveling of PEDOT:PSS can be improved with the surface treatment of P3HT:PCBM, which can also improve device performance.[39-40,59] The hydrophobic effect of the P3HT:PCBM surface can be reduced by wetting the P3HT:PCBM surface with a polar solvent that has limited solubility with P3HT:PCBM, such as isopropyl alcohol and 1-octanol.[24-25,60] Additionally, the residence time should be short to achieve good print quality of PEDOT:PSS on top of P3HT:PCBM and also to avoid a negative impact on device performance.

In the R2R rotary screen printing process described here, ink distribution is controlled by the choice of the printing screen, the pressure of the squeegee, the speed of the printing, and the drying profile. The screen printable PEDOT:PSS inks are recommended for use with polyester screens instead of metallic screens. Because the rotary screen printing unit is limited to metallic screens, the test screens were either hexagonally patterned nickel plates or woven steel threads. The structures of the test screens were developed for solid area printing with line thicknesses of 200, 215, and 305 lines/inch (=L). The wet deposit varied from 15 to 18 µm, aiming at a final film thickness close to 1 µm. As the woven screen with 200 L steel threads copies the meshwork into the printed surface, a nickel plate with 215 L hexagonal patterning provides significantly better leveling of PEDOT:PSS. A 305 L nickel plate prints the sharpest image, but reduces the uniformity within the printed areas, thus the 215 L plate gives the best printing quality. The pressure of the squeegee was set as low as possible to avoid PEDOT:PSS oozing through the screen with a 1.5-bar value. A clear influence of the web speed on the quality of printed PEDOT:PSS was not detected as the web speed ranged from 2 to 6 m min^{-1}; thus, 2 m min^{-1} was chosen to increase the efficiency of drying and the time of

leveling before hot air drying at +130°C temperature. The P3HT:PCBM surface was pre-treated with solvent before the printing of PEDOT:PSS to provide proper wetting and leveling of the ink. PEDOT:PSS layer was printed at a thickness of 1.3 (±0.1) µm, which was considered thick enough to protect the P3HT:PCBM layer from the silver paste and thin enough to avoid delamination of PEDOT:PSS.[24] As presented here, the uniform layer of PEDOT:PSS could be printed on top of P3HT:PCBM in the R2R process, despite the challenging rheology of the PEDOT:PSS and the hydrophobic surface of the P3HT:PCBM. Additionally, the R2R printing process described in this paper was repeatable, thus good printing quality was constant throughout the R2R run.

2.3. Compatibility of silver pastes

Various silver pastes were investigated in laboratory scale in terms of cell performance to determine a suitable paste for R2R processing of the conductive top electrode. Two main aspects were emphasized in the paste selection: i) compatibility of the silver paste on the underlying layers, and ii) R2R processability by means of thermal capacity limited by the size and maximum temperature of the drying units. Thermally curable silver pastes containing low amounts of acetate-based solvents were purchased from DuPont and Spraylat. The pastes PV 410 and PV 414 from DuPont and pastes XCMS-015 and XPVS-670 from Spraylat were flat-bed screen-printed on top of laboratory scale-processed small-area cells, with a defined active area of 18 mm2. The cells were fabricated using table top printers and the drying was fitted to respond to the drying efficiency in the R2R process. The effect of the silver pastes PV 410, PV 414, XCMS-015 and XPVS-670 on the electrical parameters involving open circuit voltage (VOC), short-circuit current density (JSC), and PCE is shown in Figure 3. According to current-voltage characteristics, a PCE between 2% to 3% was obtained with silver pastes PV 410, PV 414 and XPVS-670 whereas paste XCMS-015 had a PCE of only 1%. Notably, however, the performance was overestimated by the area of PEDOT:PSS, which was designed to be larger than the area of silver to avoid direct contact between the silver paste and the P3HT:PCBM layer. Because the highly conductive PEDOT:PSS also acts as a hole contact, a larger area of PEDOT:PSS can increase the cell performance by ~20%. Further, the effect of PEDOT:PSS as a hole contact will diminish as the active area of cells/modules increase. Even though PV 410 silver paste exhibited good cell performance as a hole contact, the processing of the paste was considered suitable only for flat-bed screen printer due to clogging of the screen. PV 414 silver paste was a promising candidate for R2R printing in terms of cell performance and processability. Silver paste XCMS-015 exhibited the lowest cell performance, and the current density was 30% lower compared to the other cells with a PCE just above 1%. The solvents of the silver pastes were similar. However, the lower performance with silver paste XCMS-015 could be attributed to the lower solid content of the silver paste, which resulted in a significant increase of the solvent.[24] Silver paste XPVS-670 provided the best cell

performance among the tested silver pastes with excellent printing quality and easy processability.

Based on the laboratory scale experiments, silver paste XPVS-670 was selected for fabrication of the R2R modules since it exhibited high cell performance, sufficiently low requirements for curing, and excellent processing. Rotary screen printing of XPVS-670 in R2R process was achieved with a 275 mesh metallic screen, and it was designed to provide a wet thickness of 14 μm. A printing speed of 2 m min^{-1} allowed for drying under a hot air unit at +130°C for 2 min. The following processing conditions resulted in a final layer thickness of 11 (±0.4) μm and good quality printing, which were maintained throughout the run. The dimensions of the printed structures are presented in Sections 2.4 and 2.5.

2.4. Patterning accuracy and registration

The ZnO and P3HT:PCBM materials processed with gravure printing were printed as continuous lines with a striped design on top of the patterned ITO, so only cross machine alignment (CD, perpendicular to the printing direction) required adjustment during the run. PEDOT:PSS and silver, however, were rotary screen-printed to a rectangular pattern, so these layers needed to be aligned also in the printing direction(machine direction, MD). The layout is shown in Figure 4. The layout was designed with CD overlap between the printed layers in order to obtain the serial connection between the cells through the ITO and silver layers. Thus, each layer was aligned on the previous layer except the P3HT:PCBM, that was aligned on the ITO pattern. Respectively, in the MD the PEDOT:PSS was positioned to ITO pattern and silver to PEDOT:PSS layer.

It should be noted that the pilot printing machine used for these experiments was equipped with control cameras, but registration was performed manually. Additionally, the R2R printing alignment accuracy was challenged by the detection of the highly transparent layers of ZnO and ITO. The alignment tolerance covering the influences caused by the misalignment between the printed layers and the spreading or shrinking of the wet film was designed to be at maximum 600 μm for each layer. The accuracy of the CD alignment between the printed layers was measured microscopically afterwards, and the sampling distance comprised 50 repeat lengths of R2R processed modules (Figure 5). The repeat length was defined as the circumference of the printing cylinder/screen and the repeat length of the R2R machine was 409.6 mm; thus, 50 repeat lengths corresponded to a web length of 20 meters. As mentioned earlier, ZnO and P3HT:PCBM layers were aligned with ITO whereas PEDOT:PSS was aligned with P3HT:PCBM and silver with PEDOT:PSS. The limited detection of the transparent layers increased the CD distance to the previous layer; thus, the mean dislocation of the ZnO layer was 300 μm further and periodically fluctuated. The P3HT:PCBM, PEDOT:PSS, and silver were aligned according to the specifications with few exceptions. The CD alignment of the

P3HT:PCBM layer shifted only 100 μm from the mean and, the silver layer followed the fluctuation of the PEDOT:PSS. In some cases, the layer alignment exceeded the specified tolerance, although it was compensated by the high accuracy of the alignment of the other layers (see Figure 6a).

The dimensional accuracy of the printed image is influenced by the rheology of the ink, the surface properties of the ink and substrate, the precision provided by the printing cylinder or the screen, and the processing conditions. Here, the dimensional accuracy in the CD of the printed layers (Figure 6b) was compared to the layout of the module by measuring the samples that had been introduced as the alignment of the R2R-printed modules was examined. The R2R gravure-printed ZnO layer was broadened from the designed 5.0 mm to a 5.3-mm layer due to the low viscosity of the ink and the good wetting properties on top of the ITO layer. As described earlier, the accuracy of the cell alignment of each layer was designed to be within 600 μm; nevertheless, ZnO layer spreading over the other edge of the cell was accepted up to 1000 μm. Gravure printing, however, enables excellent control of the ink, as shown by the R2R-printed P3HT:PCBM layer corresponding to a 5.6-mm width as designed in the layout of the module. Thus, the good precision achieved in the edge area of printed features is an absolute strength of gravure printing. The R2R rotary screen-printed layer of PEDOT:PSS was reduced 1% from the specified width of 5.6 mm, resulting in a final dimension of 5.5 mm. Shrinkage likely occurred during the thermal drying of the layer rather than by printing. The dimensional control of the R2R rotary screen-printed silver paste showed excellent dimensional accuracy, corresponding to a 5.8-mm width of the layout. The dimensional accuracy of the printed layers over the sampling distance of 50 repeat lengths corresponded to a mean dimension of 5.3 mm ±1.0% for ZnO (5.0 mm engraved pattern), 5.6 mm ±0.5% for P3HT:PCBM (5.6 mm engraved pattern), 5.5 mm ±1.0% for PEDOT:PSS (5.6 mm engraved pattern), and 5.8 mm ±1.0 % for silver (5.8 mm engraved pattern).

2.5. Electrical performance of the printed modules

Six sizes of printed modules by gravure printing and rotary screen printing were processed. The layout of the R2R module process is shown in Figure 7. One side of the roll comprised 8 monolithically serially connected cells and, the other side comprised 19 serially connected cells, and 3 different cell sizes were prepared (A=0.34 x 5.0 cm^2, B=0.34 x 10.0 cm^2 and C=0.34 x 15 cm^2). Thus, the total active area of the modules varied from 13.6 cm^2 to 96.5 cm^2.

The surface morphologies of the P3HT:PCBM, PEDOT:PSS, and silver were measured with atomic force microscopy and topography images of the samples are shown together with optical microscopy images in Figure 8. R2R gravure printing of P3HT:PCBM provided a smooth and uniform surface with the root mean square roughness (Rq) value of 1.45 nm and a maximum height variation (peak-to-valley) of 13 nm on a

cross-section of the image. The rheological properties of P3HT:PCBM ink favored a balanced transfer and leveling of the ink, leading to good printed film formation. The optimal drying profile was not examined in this work, and thus the morphology might be improved by optimizing the heat transfer conditions during film formation. The topography image of the R2R rotary screen-printed PEDOT:PSS layer has an Rq of 23.6 nm and a height variation of 0.2 µm on a cross-section of the image. These values are higher than P3HT:PCBM due to the rheological properties of the PEDOT:PSS ink and the type of printing screen. As explained earlier, the rheology of PEDOT:PSS indicates a potential risk with respect to uneven ink distribution and limited leveling. Additionally, the ink and target layer thickness define the mesh and emulsion thickness of the screen, and thus have a major impact on the quality of the printed layer together with the process parameters. Because the mean layer thickness of PEDOT:PSS was 1.3 µm and the height variation was 0.2 µm, the result was acceptable. The silver layer shows an agglomerated surface topography structure with a surface roughness of 655 nm and a height variation ~3.1 µm on a cross-section of the image. The agglomerates contained smaller entities with a diameter of ~400 nm referring to the particle size of the silver.

A total of 220 printed modules were electrically characterized. No thermal post treatment or light soaking was used for the modules prior to the current-voltage measurements. Mean efficiencies ranged from 1.7% to 1.8%, while the maximum values exceeded 2.0% to 2.2% depending on the module size. This shows the excellent repeatability of the R2R printing of the modules. Additionally, we investigated repeatability by characterizing two series of modules with 19 serially connected cells. The first test series contained 36 modules of repeat lengths of 8-19, and the second series contained 36 modules of repeat lengths of 38-49. Both series of modules were consecutive modules from the R2R-produced roll in three different module sizes. The short circuit current (ISC), VOC, fill factor (FF), and PCE of the modules is depicted in Figure 9. The parameters for the repeat lengths of 8-19 (series 1) are indicated with filled circles and the repeat lengths of 38-49 (series 2) are indicated with open circles. The module size of A19 refers to the total active area of 32.2 cm^2, B19 to 64.4 cm^2, and C19 to 96.5 cm^2.

Small fluctuations were observed for the short circuit current values. The variation correlated with the manually operated registration, which affects the size of each cell in all sizes of modules printed at the same time, and consequently the short circuit current values as well. The CD variation of 100 µm will change the area of the cell with the largest module (C19) by 3%. This means that a variation of 100 to 200 µm will affect the short circuit current value by ±1-2 mA. The mean electrical parameters of the test series are summarized in Table 1.

The mean value is calculated as an average of both test series shown in Figure 9. Jsc per cell is calculated by dividing the

short circuit current density by the area of the one cell in the module structure.

If the registration was aligned as in the design, the width of the cell in all 19 cell module sizes should be 3.4 mm. The gap between the ITO patterns was 2.0 mm. Based on the design, the length of the cells with A19 was 50 mm, B19 100 mm, and C19 150 mm. The mean PCE remained at a rather constant level during processing, from 1.7% to 1.8% (Table 1). This implies that uniform printing quality of the different layers is maintained through the run. Because all the modules taken to the test series functioned properly, there were no detrimental processing defects that could be detected such as shorted cells.

The Voc of the modules ranged from 10.9 V to 11.1 V. The number of cells in a series connection was the same in all module sizes investigated, so the Voc should not vary. The short circuit current is directly proportional to the active area. The B19 module had double the length of A19 and a two-fold greater mean short circuit current value. With the largest module size, C19, the values were similar although the mean short circuit current was 3% lower (compared A19 with to three-fold higher value).

Conclusions

R2R-printed inverted OPV modules were fabricated with gravure printing and rotary screen printing processes which allow 2D patterning. The rheological properties of the inks and their relation to printability, the compatibility of the silver paste with the device, and the process limits were examined to define the parameters for each process step. R2R processing produced a large amount of information as the morphology of the R2R-printed layers, the cross machine accuracy of the printed pattern and registration, the repeatability of the R2R fabrication process, and the influence of registration on the module performance were studied. As an outcome, we fabricated R2R-printed OPV modules with an active area up to 96.5 cm^2 in size achieving good surface properties of the printed layers, good processing control, and a mean power conversion efficiency of 1.8% with uniform quality. To the best of our knowledge, this is the first report of printed OPV modules using the R2R gravure and screen printing processes, and the data presented here increase our understanding in terms of processing and patterning of OPV structures as the module layout is changed into arbitrary shapes and sizes.

Experimental

The printed OPV modules were constructed on top of ITO-coated PET roll purchased from Solutia/Eastman (40-60 Ω sq^{-1}). The PET and ITO thicknesses were 125 µm and 0.125 µm, respectively. As a first process step, the ITO was patterned with Isishape HiperEtch 09S Type 40 paste (Merck) as an negative image to the desired pattern. R2R rotary screen printing was performed with a printing speed of 1.1 m min^{-1}. After printing, the printed film continued directly into the R2R

hot air drying units set to a temperature of 140°C for 218 s. The paste was washed off in baths of water and 2-propanol. After patterning, the surface was ultrasonically washed and dried in the R2R process. ZnO nanoparticle suspension in ethanol (Nanograde, Switzerland) was used for the electron transport layer. The ZnO layer was R2R gravure-printed and dried at 140°C for 30 s (hot air drying). The details of the R2R gravure printing of ZnO is presented in a separate article by Vilkman *et al.*[55] Regioregular P3HT (#4002-E, Rieke Metals) was used as the donor, and PCBM [C60] (purity 99.5 %, Nano-C) as the acceptor in the photoactive blend. Both were received as solid materials and dissolved in 1.2-dichlorobenzene to a total concentration of 0.13 g ml^{-1}. In addition, the photoactive layer was deposited by R2R gravure printing. The printing speed was 8 m min^{-1} and the applied nip pressure was 1 bar. The printing cylinder contained engravings with a line density of 120 lines cm^{-1}. High viscous PEDOT:PSS (Agfa, EL-P 5015) was R2R rotary screen-printed. Preliminary tests were performed using GV screen with 200L mesh from Gallus and rotaplate screens 215V and 305V from Stork. Fabrication of the modules was achieved with a Stork rotaplate 215V screen. The printing speed was 2 m min^{-1}. The hot air drying units were set to 130°C with a total drying time of 120 s. Compatibility of the silver paste was tested using four thermally curable pastes: PV 410 and PV 414 from DuPont and, XCMS-015 and XPVS-670 from Spraylat with a flat-bed screen printer in laboratory scale. XPVS-670 heat curable silver paste was chosen as the hole contact in the inverted module configuration. R2R rotary screen printing was performed with a 275 L steel mesh screen (RVS) from Gallus. The printing speed was 2 m min^{-1}. The drying temperature was 130°C with a total drying time of 120 s.

Characterization

The rheology of the PEDOT:PSS and P3HT:PCBM inks was measured using an MCR-301 rheometer (Anton Paar). The alignment and dimensions of the printed layers were measured using a Smartscope OGP-250 microscope, and the layer thicknesses were measured with a Dektak profilometer (Veeco). The surface morphologies of the P3HT:PCBM, PEDOT:PSS, and silver were measured using a Veeco Dimension 3100 in tapping mode. A high quality silicon tip with a radius less than 10 nm was used to probe the sample surfaces. After R2R processing, the non-encapsulated modules were transferred to glove box for current-voltage measurements. The modules did not undergo any light soaking or thermal treatment after R2R processing prior to electrical characterization. The current-voltage characteristics under illumination were measured with a solar simulator (Atlas SolarCellTest 1200) calibrated to 100 mW cm^{-2} using a calibrated Si-reference cell filtered with a KG5 filter. The active area was defined by the overlap of ITO bottom and Ag top electrodes.

References

1   C. W. Tang, *Appl. Phys. Lett.*, 1986, **48**, 183.

2   G. A. Chamberlain, *Sol. Cells,* 1983, **8**, 47.

3   M. C. Scharber, D. Mühlbacher, M. Koppe, P. Denk, C. Waldauf, A. J. Heeger, C. J. Brabec, *Adv. Mater.*, 2006, **18**, 789.

4   J. You, L. Dou, K. Yoshimura, T. Kato, K. Ohya, T. Moriarty, K. Emery, C. C. Chen, J. Gao, G. Li, Y. Yang, *Nat. Commun.*, 2013, **4**, 1446.

5   N. Espinosa, R. García-Valverde, A. Urbina, F. Lenzmann, M. Manceau, D. Angmo, F. C. Krebs, *Sol. Energy Mater. Sol. Cells,* 2012, **97**, 3.

6   N. Espinosa, R. Garcia-Valverde, A. Urbina, F. C. Krebs, *Sol. Energy Mater. Sol. Cells*, 2011, **95**, 1293.

7   N. Espinosa, R. García-Valverde, F. C. Krebs, *Energy Environ. Sci.*, 2011, **4**, 1547.

8   M. Jørgensen, J. E. Carlé, R. R. Søndergaard, M. Lauritzen, N. A. Dagnæs-Hansen, S. L. Byskov, T. R. Andersen, T. T. Larsen-Olsen, A. P. L. Böttiger, B. Andreasen, L. Fu, L. Zuo, Y. Liu, E. Bundgaard, X. Zhan, H. Chen, F. C. Krebs, *Sol. Energy Mater. Sol. Cells*, 2013, **119**, 84.

9   R. R. Søndergaard, M. Hösel, F. C. Krebs, *J. Polym. Sci., Part B: Polym. Phys.*, 2013, **51**, 16.

10   S. Dongaonkar, S. Loser, E. J. Sheets, K. Zaunbrecher, R. Agrawal, T. J. Marks, M. A. Alam, *Energy Environ. Sci.*, 2013, **6**, 782.

11   R. Po, A. Bernardi, A. Calabrese, C. Carbonera, G. Corso, A. Pellegrino, *Energy Environ. Sci.*, 2014, **7**, 925.

12   S. B. Darling, F. You, *RSC Adv.*, 2013, **3**, 17633.

13   F. C. Krebs, M. Jørgensen, *Sol. Energy Mater. Sol. Cells*, 2013, **119**, 73.

14   T. P. Osedach, T. L. Andrew, V. Bulovic, *Energy Environ. Sci.*, 2013, **6**, 711.

15   R.Po, G.Bianchi, C.Carbonera, A.Pellegrino, *Macromolecules*, 2015, **48**, 453.

16   W. Chen, T. Xu, F. He, W. Wang, C. Wang, J. Strzalka, Y. Liu, J. Wen, D. J. Miller, J. Chen, K. Hong, L. Yu, S. B. Darling, *Nano Lett.*, 2011, **11**, 3707, DOI 10.1021/nl201715q.

17   B. A. Collins, J. R. Tumbleston, H. Ade, *J. Phys. Chem. Lett*, 2011, **2**, 3135.

18   C. Koidis, S. Logothetidis, A. Ioakeimidis, A. Laskarakis, C. Kapnopoulos *Org. Electron.*, 2013, **14**, 1744.

19   C. Koidis, S. Logothetidis, S. Kassavetis, C. Kapnopoulos, P. G. Karagiannidis, D. Georgiou, A. Laskarakis, *Sol. Energy Mater. Sol. Cells,* 2013, **112**, 36.

20   W.-H. Baek, H. Yang, T.-S. Yoon, C. J. Kang, H. H. Lee, Y.-S. Kim Sol., *Energy Mater. Sol. Cells,* 2009, **93**, 1263.

21   R. Søndergaard, M. Hösel, D. Angmo, T. T. Larsen-Olsen, F. C., *Krebs Mater. Today,* 2012, **15**, 36.

22   L. Blankenburg, K. Schultheis, H. Schache, S. Sensfuss, M. Schrödner, *Sol. Energy Mater. Sol. Cells,* 2009, **93**, 476.

23   F. C. Krebs, S. A. Gevorgyan, J. Alstrup, *J. Mater. Chem.,* 2009, **19**, 5442.

24   F. C. Krebs, T. Tromholt, M. Jorgensen, *Nanoscale,* 2010, **2**, 873.

25   F. C. Krebs, J. Fyenbo, M. Jorgensen, *J. Mater. Chem.,* 2010, **20**, 8994.

26 Y. Galagan, I. G. de Vries, A. P. Langen, R. Andriessen, W. J. H. Verhees, S. C. Veenstra, J. M. Kroon*, Chem. Eng. Process. Process Intensif.,* 2011, **50**, 454.

27 D. Angmo, S. A. Gevorgyan, T. T. Larsen-Olsen, R. R. Søndergaard, M. Hösel, M. Jørgensen, R. Gupta, G. U. Kulkarni, F. C. Krebs*, Org. Electron.,* 2013, **14**, 984.

28 M. Hösel, R. R. Søndergaard, M. Jørgensen*, F. C. Krebs, Energy Technol.,* 2013, **1**, 102.

29 F. C. Krebs, M. Hösel, M. Corazza, B. Roth, M. V. Madsen, S. A. Gevorgyan, R. R. Søndergaard, D. Karg, M. Jørgensen*, Energy Technol.,* 2013, **1**, 378.

30 F. C. Krebs, N. Espinosa, M. Hösel, R. R. Søndergaard, M. Jørgensen*, Adv. Mater.,* 2014, **26**, 29.

31 P. Sommer-Larsen, M. Jørgensen, R. R. Søndergaard, M. Hösel, F. C. Krebs*, Energy Technol.,* 2013, **1**, 15.

32 T.R. Andersen, H. F. Dam, M. Hösel, M. Helgesen, J.E. Carlé, T.T. Larsen-Olsen, S.A. Gevorgyan, J.W. Andreasen, J. Adams, N. Li, F. Machui, G.D. Spyropoulos, T. Ameri, N. Lemaître, M. Legros, A. Scheel, D. Gaiser, K. Kreul, S. Berny, O. R. Lozman, S. Nordman, M. Välimäki, M. Vilkman, R.R. Søndergaard, M. Jørgensen, C. J. Brabec, F. C. Krebs, *Energy Environ. Sci.,* 2014 7,2925.

33 D. Angmo, J. Sweelssen, R. Andriessen, Y. Galagan, F. C. Krebs, *Adv. Energy Mater.*, 2013, 3, 1230.

34 Y. Galagan, E. W. C. Coenen, B. Zimmermann, L. H. Slooff, W. J. H. Verhees, S. C. Veenstra, J. M. Kroon, M. Jørgensen, F. C. Krebs, R. Andriessen*, Adv. Energy Mater.,* 2014, **4**, DOI 10.1002/aenm.201300498.

35 T. M. Eggenhuisen, Y. Galagan, A. F. K. V. Biezemans, T. M. W. L. Slaats, W. P. Voorthuijzen, S. Kommeren, S. Shanmugam, J. P. Teunissen, A. Hadipour, W. J. H. Verhees, S. C. Veenstra, M. J. J. Coenen, J. Gilot, R. Andriessen, W. A. Groen, *J. Mater. Chem. A*, 2015, **3**, 7255-7262

36 J. M. Ding, A. de la Fuente Vornbrock, C. Ting, V. Subramanian, Sol. Energy Mater. Sol. Cells, 2009, **93**, 459.

37 P. Kopola, T. Aernouts, S. Guillerez, H. Jin, M. Tuomikoski, A. Maaninen, J. Hast*, Sol. Energy Mater. Sol. Cells,* 2010, **94**, 1673.

38 P. Kopola, T. Aernouts, R. Sliz, S. Guillerez, M. Ylikunnari, D. Cheyns, M. Välimäki, M. Tuomikoski, J. Hast, G. Jabbour, R. Myllylä, A. Maaninen, Sol. Energy Mater. Sol. Cells, 2011, 95, 1344.

39 M. M. Voigt, R. C. I. Mackenzie, C. P. Yau, P. Atienzar, J. Dane, P. E. Keivanidis, D. D. C. Bradley, J. Nelson*, Sol. Energy Mater. Sol. Cells,* 2011, **95**, 731.

40 M. M. Voigt, R. C. I. Mackenzie, S. P. King, C. P. Yau, P. Atienzar, J. Dane, P. E. Keivanidis, I. Zadrazil, D. D. C. Bradley, J. Nelson Sol*., Energy Mater. Sol. Cells,* 2012, **105**, 77.

41 J. Yang, D. Vak, N. Clark, J. Subbiah, W. W. H. Wong, D. J. Jones, S. E. Watkins, G. Wilson, *Sol. Energy Mater. Sol. Cells,* 2013, **109**, 47.

42 P. Apilo, J. Hiltunen, M. Välimäki, S. Heinilehto, R. Sliz, J. Hast, *Prog. Photovoltaics*, 2014, DOI 10.1002/pip.2508.

43 A. Hübler, B. Trnovec, T. Zillger, M. Ali, N. Wetzold, M. Mingebach, A. Wagenpfahl, C. Deibel, V. Dyakonov, *Adv. Energy Mater.*, 2011, **1**, 1018.

44 R. Po, C. Carbonera, A. Bernardi, F. Tinti, N. Camaioni, *Sol. Energy Mater. Sol. Cells* 2012, 100, 97.

45 D.S. Hecht, L. Hu, G. Irvin, *Adv. Mater* 2011, 23, 1482.

46 T.R. Andersen, H. F. Dam, B. Andreasen, M. Hösel, M. V. Madsen, S. A. Gevorgyan, R. R. Søndergaard, M. Jørgensen, F. C. Krebs, *Sol. Energy Mater. Sol. Cells* 2014, 120, 735.

47 Y. Galagan, E.W.C. Coenen, S. Sabik, H. H. Gorter, M. Barink, S.C. Veenstra, J. M. Kroon, R. Andriessen, P. W. M Blom, *Sol. Energy Mater. Sol. Cells*, 2012, **104**, 32.

48 J-S. Yu, I. Kim, J-S Kim, J. Jo, T.T. Larsen-Olsen, R.R. Søndergaard, M. Hösel, D. Angmo, M. Jørgensen, F.C. Krebs, *Nanoscale*, 2012, **4**, 6032.

49 P. Kopola P, B. Zimmermann, A. Filipovic, H-F. Schleiermacher, J. Greulich, S. Rousu, J. Hast, R. Myllylä, U. Würfel, *Sol. Energy Mater. Sol. Cells*, 2012, **107**, 252.

50 H.J. van de Wiel, Y. Galagan, T.J. van Lammeren, J. F. J de Riet, J. Gilot, M.G.M. Nagelkerke, R.H.C.A.T. Lelieveld, S. Shanmugam, A. Pagudala, D. Hui, W.A. Groen, *Nanotechnology*, 2013, **24**, 484014-1.

51 D. Kaduwal, H-F. Schleiermacher, J. Schulz-Gericke, T. Kroyer, B. Zimmermann, U. Würfel, *Sol. Energy Mater. Sol. Cells 2014*, **124**, 92.

52 G.A. dos Reis Benatto, B. Roth, M.V. Madsen, M. Hösel, R.R. Søndergaard, M. Jørgensen, F. C. Krebs, *Adv. Energy Mater.*, 2014, **4**, 1400732.

53 F. Guo, N. Li, V. V. Radmilović, V. R. Radmilović, M. Turbiez, E. Spiecker, K. Forberich, C. J. Brabec, *Energy Environ. Sci.*, 2015, DOI: 10.1039/c5ee00184f

54 M. Ylikunnari, J. Hiitola-Keinänen, E. Jansson, S. Rousu, *Proc. of LOPE-C Conf. Roll-to-roll patterning of electrodes*, Munich, Germany ((6, 2012)).

55 M. Vilkman, P. Apilo, M. Välimäki, M. Ylikunnari, A. Bernardi, R. Po, G. Corso, J. Hast, *Energy Technol.,* 2015, DOI 10.1002/ente.201402155.

56 R. Kitsomboonloha, S. J. S. Morris, X. Rong, V. Subramanian, *Langmuir*, 2012, **28**, 16711.

57 F. C. Krebs, *Sol. Energy Mater. Sol. Cells*, 2009, **93**, 465.

58 F. J. Lim, K. Ananthanarayanan, J. Luther, G. W. Ho, *J. Mater. Chem.*, 2012, **22**, 25057.

59 S.-A. Gopalan, M.-H. Seo, G. Anantha-Iyengar, B. Han, S.-W. Lee, D.-H. Kwon, S.-H. Lee, S.-W. Kang, *J. Mater. Chem. A,* 2014, **2**, 2174.

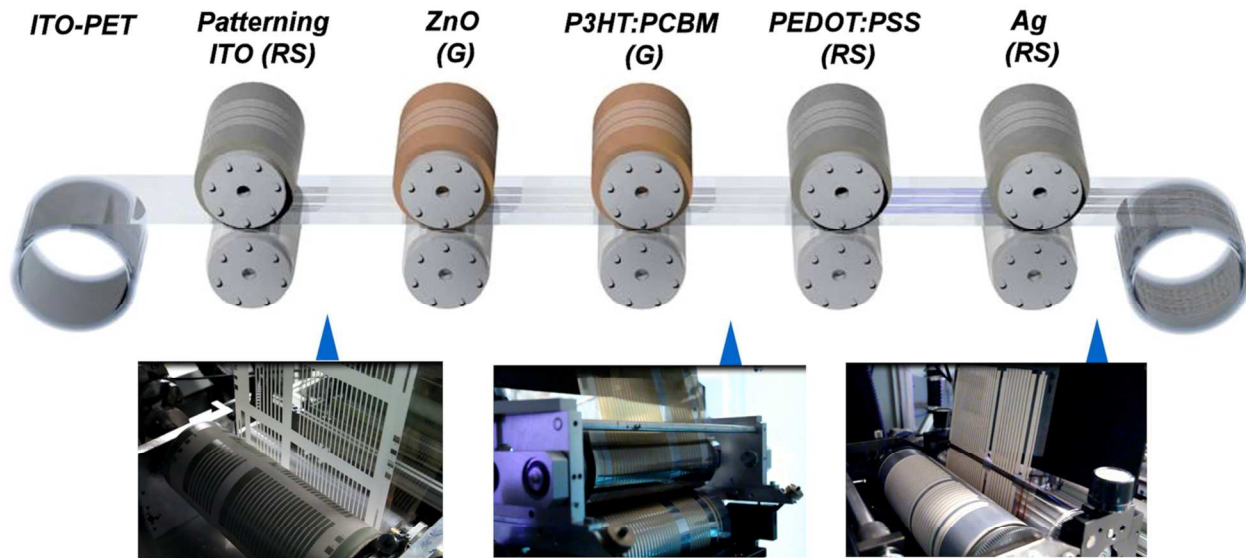60 F. C. Krebs, *Org. Electron.*, 2009, **10**, 761.

Figure 1. R2R process of printed inverted OPV modules. Used printing methods for separated OPV layers are abbreviated as RS= rotary screen printing, G=gravure printing.

Ink	1 s⁻¹	100 s⁻¹	1000 s⁻¹	6000 s⁻¹
PEDOT:PSS	104.0 Pa•s	5.6 Pa•s	1.7 Pa•s	0.6 Pa•s
P3HT:PCBM (130 mg/ml in o-DCB)	43.3 mPa•s	26.0 mPa•s	24.9 mPa•s	24.8 mPa•s
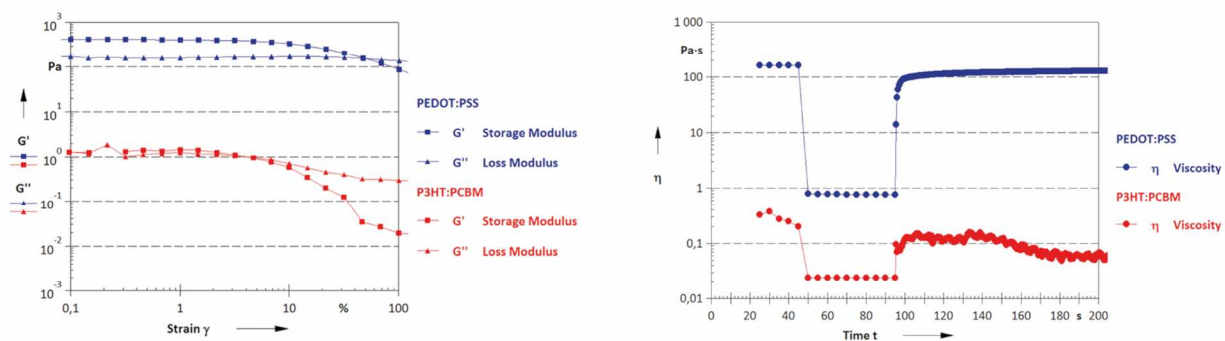
Figure 2. Amplitude sweep (left) and thixotropic behaviour (right) of PEDOT:PSS (blue) and P3HT:PCBM (red) inks. Amplitude sweep was performed using strain levels from 0.1% to 100%. The flow point is the crossing point of G' and G'' curves. In the thixotropy test, the initial and final shear rates were 0.5-1 s⁻¹ and the high shear rate was 4000-6000 s⁻¹. Higher shear rate values were used for lower viscosity active ink.
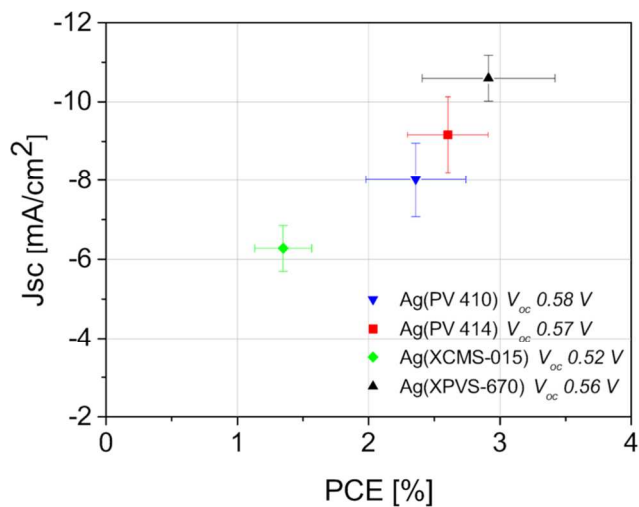
Figure 3. Comparison of organic solar cells produced with four different silver paste products. The performance of the laboratory scale printed cells is presented in terms of the open circuit voltage and the current density with the power conversion efficiency.
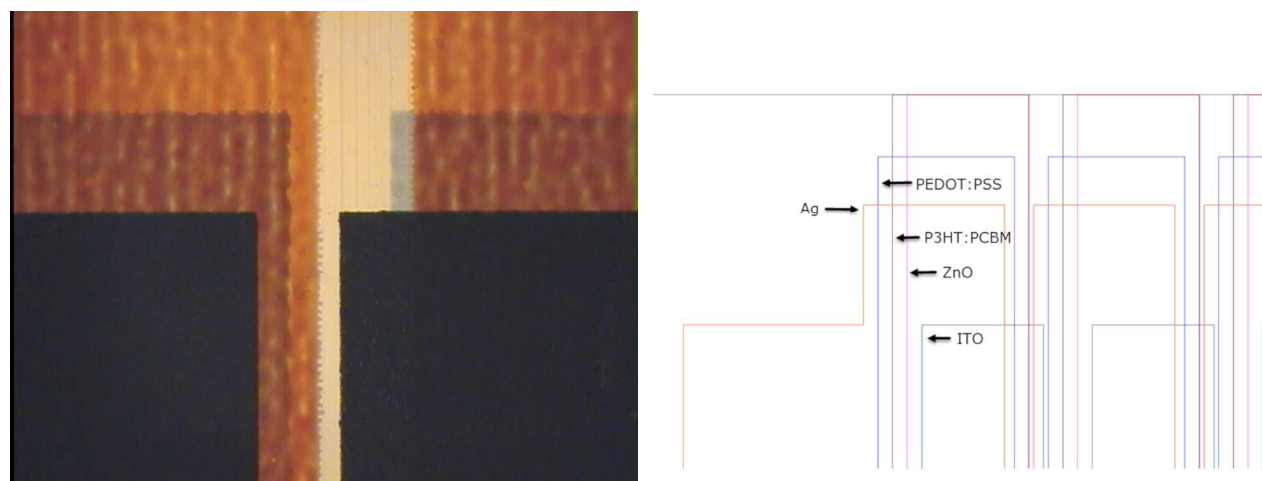

Figure 4. The serially connected OPV module where the layers from the left are as: ITO, ZnO, P3HT:PCBM, PEDOT:PSS and silver.

Figure 5. R2R fabricated printed inverted OPV modules using gravure printing and rotary screen printing techniques.
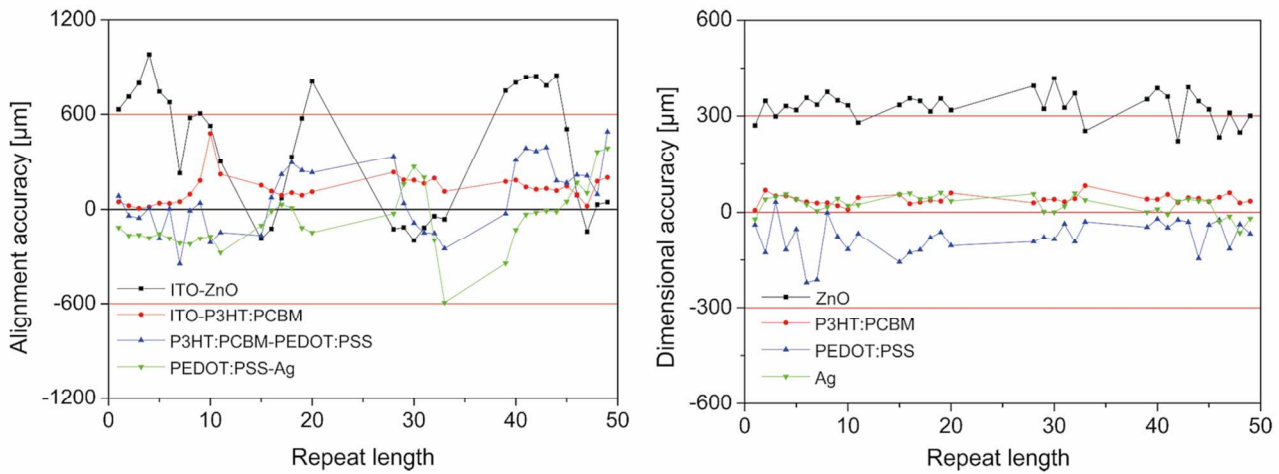

Figure 6. Cross machine direction profile of the alignment (left side) and dimensions (right side) of R2R gravure-printed (ZnO, P3HT:PCBM) and rotary screen-printed (PEDOT:PSS, silver) layers of the OPV module showing the deviation the nominal value (ZnO and P3HT:PCBM with a respect to ITO, PEDOT:PSS with a respect to P3HT:PCBM and silver with a respect to PEDOT:PSS.
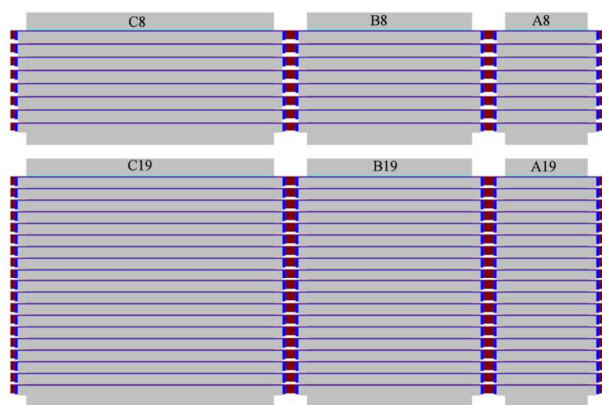
Figure 7. Layouts of the printed modules in the R2R process. A refers to the shortest module (5 cm), B to the medium length module (10 cm), and C to the longest module (15 cm). The number 8 refers to 8 monolithically series connected cells, and the number 19 refers to 19 monolithically series connected cells.
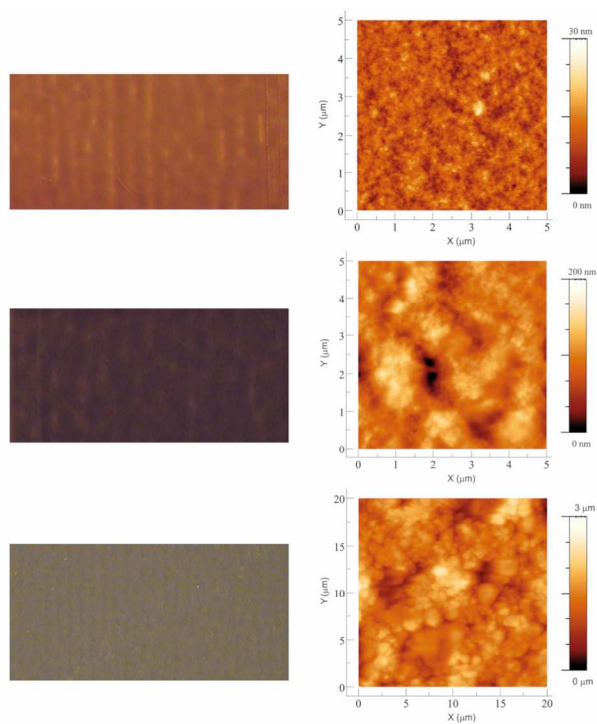

Figure 8. Optical microscopic images with a magnification of 38 (a, c, and e, respectively) and AFM topographies of P3HT:PCBM, PEDOT:PSS, and silver layers (b, d, and f, respectively). The x-direction of the AFM image is parallel to the machine direction and y-direction parallel to the cross machine direction of the printing.
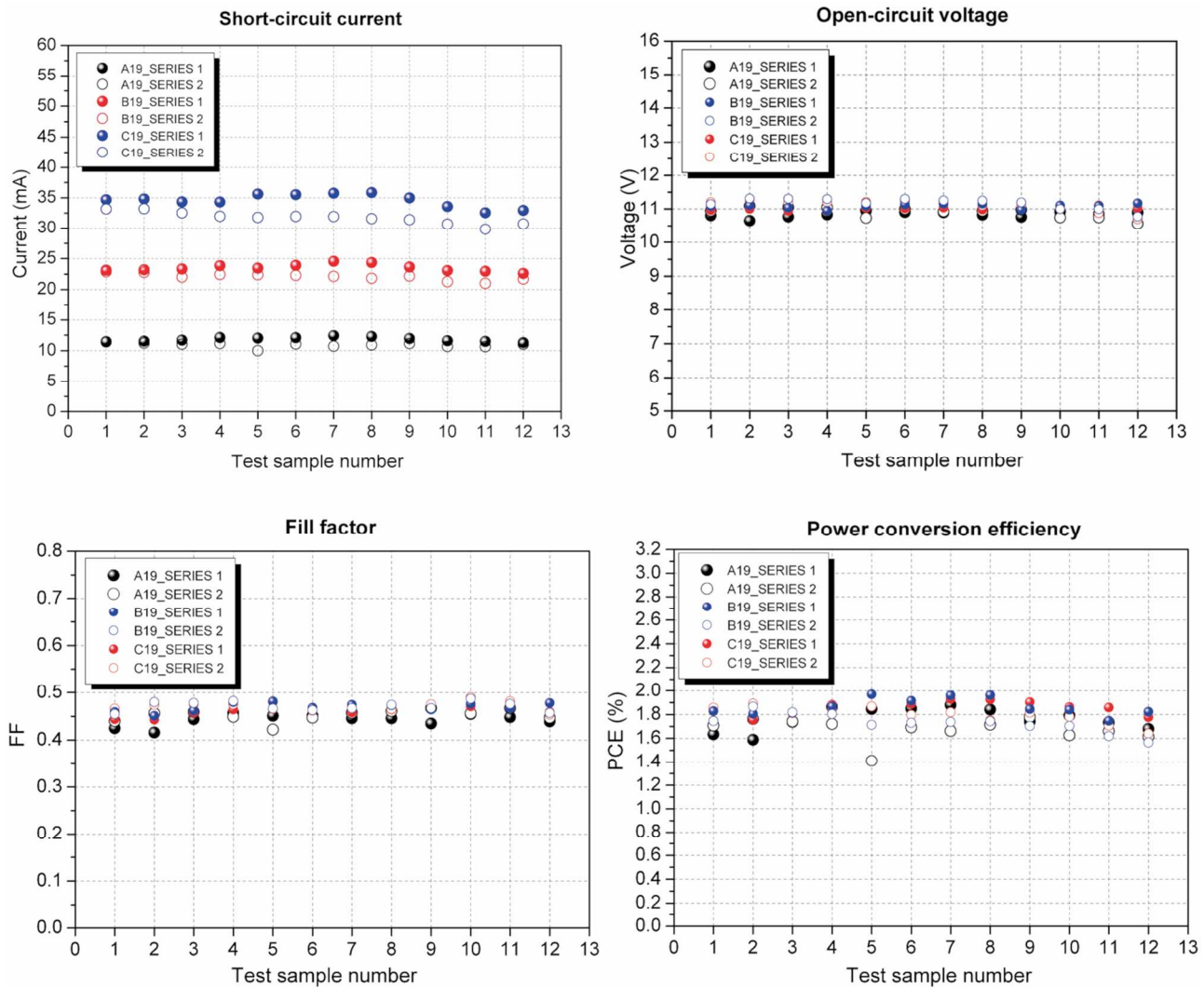
Figure 9. (a) Short circuit current density, (b) open-circuit voltage, (c) fill factor, and (d) power conversion efficiency of fully R2R-printed modules. Two test series of three different module sizes (A19= 32.2 cm2, B19=64.4 cm2 and C19=96.5 cm2) are depicted as a function of the test sample number. The parameters for the repeat lengths of 8-19 (series 1) are shown with filled circles and the repeat lengths of 38-49 (series 2) with open circles.

TOC

R2R fabrication of inverted OPV modules using gravure and rotary screen printing techniques showing the potential of the direct 2D printing in the patterning of arbitrarily shaped and sized features.

Nanoscale Accepted Manuscript

Table 1. Mean electrical parameters for three different module sizes (A19=32.2 cm², B19=64.4 cm², and C19=96.5 cm²). The mean value is calculated as an average of both test series shown in Figure 6. Jsc per cell is calculated by dividing the short circuit current density by the area of the one cell in the module structure.

Module area	Yield	Mean Isc [mA]	Mean Jsc per cell [mA/cm²]	Mean Voc [V]	Mean Voc per cell [V]	Mean Pmpp [mW]	Mean FF	Mean PCE [%]	Max PCE [%]
32.2 cm² (A19)	100% (24/24)	11.39 (±0.59)	6.72	10.87 (±0.13)	0.57	55.40 (±3.40)	0.45 (±0.01)	1.72 (±0.11)	1.88
64.4 cm² (B19)	100% (24/24)	22.80 (±0.92)	6.73	11.06 (±0.13)	0.58	117.59 (±4.61)	0.47 (±0.01)	1.83 (±0.07)	1.93
96.5 cm² (C19)	100% (24/24)	33.16 (±1.78)	6.53	11.13 (±0.13)	0.59	173.44 (±9.88)	0.47 (±0.01)	1.80 (±0.10)	1.97